

Convergent iLQR for Safe Trajectory Planning and Control of Legged Robots

James Zhu, J. Joe Payne, and Aaron M. Johnson

Abstract—In order to perform highly dynamic and agile maneuvers, legged robots typically spend time in underactuated domains (e.g. with feet off the ground) where the system has limited command of its acceleration and a constrained amount of time before transitioning to a new domain (e.g. foot touch-down). Meanwhile, these transitions can have instantaneous, unbounded effects on perturbations. These properties make it difficult for local feedback controllers to effectively recover from disturbances as the system evolves through underactuated domains and hybrid impact events. To address this, we utilize the fundamental solution matrix that characterizes the evolution of perturbations through a hybrid trajectory and its 2-norm, which represents the worst-case growth of perturbations. In this paper, the worst-case perturbation analysis is used to explicitly reason about the tracking performance of a hybrid trajectory and is incorporated in an iLQR framework to optimize a trajectory while taking into account the closed-loop convergence of the trajectory under an LQR tracking controller. The generated convergent trajectories are able to recover more effectively from perturbations, are more robust to large disturbances, and use less feedback control effort than trajectories generated with traditional optimization methods.

I. INTRODUCTION

Legged robotics research has been increasingly focused on enabling highly dynamic and agile motions such as jumping, leaping, and landing [1–4]. Implementing these capabilities reliably would improve legged robot performance in applications such as extraterrestrial exploration and urban environment navigation where jumping up on ledges or leaping across chasms may be necessary. However, jumping and leaping are dangerous maneuvers, with failure often resulting in catastrophic outcomes for the robot.

A strategy that has been used to enable these dynamic yet precarious behaviors is leveraging highly accurate, complex models and full-body trajectory optimization to plan precise motions [3,5]. While these methods incorporate feedback controllers to stabilize the generated trajectories, there has been little focus on how these feedback controllers should be designed along with planned trajectories to stabilize closed-loop systems under error and uncertainty. This paper contributes a trajectory planning method for hybrid systems that accounts for the closed-loop performance of a given feedback controller.

Ample work has been done to study robust trajectory planning for smooth systems, with some recent results being adapted to hybrid systems like legged robots. Significant

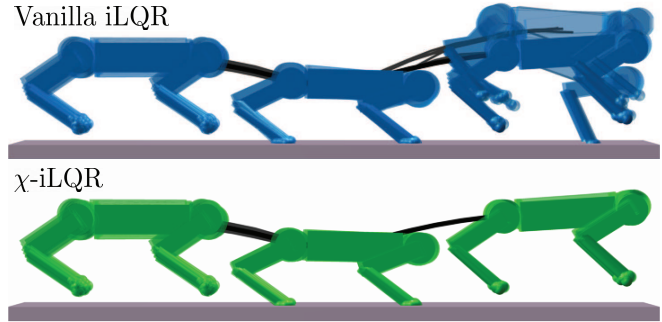


Fig. 1. Qualitatively similar quadruped gaits tracked with equivalent LQR controllers display enormous differences in final tracking performance. This figure shows results for 50 paired trials of trajectories sampled from an initial error covariance of 10^{-2} in all directions. The top blue trajectory was generated with a standard (vanilla) iLQR algorithm, while the bottom green trajectory was generated with our novel χ -iLQR, which improves the average closed-loop convergence by 92%. Note that the horizontal distance between the displayed frames is exaggerated for visual clarity. This figure only represents the convergence of the position states, and does not indicate convergence of the velocity states.

research has focused on optimizing over uncertainties in system dynamics, such as unknown disturbances and modelling errors [6–8]. These methods plan trajectories under the anticipation of some worst-case or average-case disturbance sequence. For example, [6] designed robust closed-loop trajectories for smooth systems by optimizing the volume reduction of an ellipsoidal disturbance set. Risk-sensitive planning and control is an alternate method that optimizes over the variance of a cost distribution that evolves through the trajectory [9,10]. Other approaches presented trajectory optimization algorithms for legged robots over uncertain terrain [11] and computed a forward reachable set to bound closed-loop errors [12].

Many works have quantified the stability or convergence properties of a system. A very popular method is Lyapunov analysis, where a positive definite differentiable scalar function with negative definite derivatives, called the Lyapunov function, can guarantee asymptotic stability of the system [13]. While effective, Lyapunov functions can be difficult to compute, particularly for hybrid systems, and can require methods such as sum-of-squares [14] or machine learning [15] to be tractable. A similar strategy known as the control barrier function restricts the system from entering some set of undesirable states, thus guaranteeing safety, and has been successfully implemented on legged robot hardware [16].

A different strategy to analyze the stability and conver-

This material is based upon work supported by the National Science Foundation under grant #CMMI-1943900.

All authors are with the Department of Mechanical Engineering, Carnegie Mellon University, Pittsburgh, PA, USA, jameszhu@andrew.cmu.edu, amjl@andrew.cmu.edu

gence of trajectories is contraction analysis [17], which tracks the distance between two close trajectories. If this distance monotonically decreases over the trajectory, then the system is contractive and asymptotic stability can be guaranteed. [17]. Contraction analysis has been incorporated into path planning and trajectory optimization algorithms on smooth systems [18,19]. Extending contraction analysis to hybrid systems is difficult because many mechanical hybrid systems are not contractive at hybrid events [20]. Underactuation can also make contraction impossible due to the lack of control in some directions. [21] loosened the contraction criterion and presented a method to optimize the stability of open-loop periodic orbits using monodromy matrix analysis. Here, we extend that work by generalizing to non-periodic trajectories under LQR feedback control.

This paper presents a novel adaptation of the iLQR trajectory optimization algorithm that improves closed-loop convergence under an equivalent feedback controller (i.e. without changing the LQR controller weights), see Fig. 1. Our results on simulated robots show that the presented convergent iLQR (χ -iLQR) achieves three simultaneous improvements over standard iLQR: superior tracking performance from initial perturbations, reduced feedback control effort over the trajectory, and improved robustness to large initial errors. Compared to existing methods, χ -iLQR has two key strengths. Firstly, it is based on an analysis that is simple to compute compared to methods such as sum-of-squares. Additionally, χ -iLQR captures the local tracking performance of a closed-loop trajectory, which directly predicts experimental results.

II. UNDERACTUATED HYBRID SYSTEMS

Legged robots navigate trajectories that are both hybrid and underactuated, which doubly contribute to the difficulty that exists in controlling these systems. In this section, we formally define the two terms and discuss how they can cause naive feedback controllers to underperform.

A. Hybrid Systems

Hybrid systems are a class of dynamical systems that consist of continuous domains connected by hybrid events [22,23]. Following the adaptation of [24] in [21], we define a C^r hybrid dynamical system for continuity class $r \in \mathbb{N}_{>0} \cup \{\infty, \omega\}$ as a tuple $\mathcal{H} := (\mathcal{J}, \Gamma, \mathcal{D}, \mathcal{F}, \mathcal{G}, \mathcal{R})$ where:

- 1) $\mathcal{J} := \{I, J, \dots, K\} \subset \mathbb{N}$ is the set of discrete modes.
- 2) $\Gamma \subset \mathcal{J} \times \mathcal{J}$ is the set of discrete transitions forming a directed graph structure over \mathcal{J} .
- 3) $\mathcal{D} := \coprod_{I \in \mathcal{J}} D_I$ is the collection of domains D_I .
- 4) $\mathcal{F} := \coprod_{I \in \mathcal{J}} F_I$ is a collection of time-varying vector fields with control inputs, $F_I : \mathbb{R} \times D_I \times U_I \rightarrow TD_I$, where U_I is the space of allowable control inputs.
- 5) $\mathcal{G} := \coprod_{(I,J) \in \Gamma} G_{(I,J)}(t)$ is a collection of guards where $G_{(I,J)}(t) \subset D_I \times U_I$ for each $(I, J) \in \Gamma$ is defined as a sublevel set of a C^r function, i.e. $G_{(I,J)}(t) = \{(x, u) \in D_I \times U_I \mid g_{(I,J)}(t, x, u) \leq 0\}$.

- 6) $\mathcal{R} : \mathbb{R} \times \mathcal{G} \rightarrow \mathcal{D}$ is a C^r map called the reset map that restricts as $R_{(I,J)} := \mathcal{R}|_{G_{(I,J)}(t)} : G_{(I,J)}(t) \rightarrow D_J$ for each $(I, J) \in \Gamma$.

An execution of a hybrid system [24] begins at an initial state $x_0 \in D_I$. With input $u_I(t, x)$, the system obeys the dynamics F_I on D_I . If the system reaches guard surface $G_{(I,J)}$, the reset map $R_{(I,J)}$ is applied and the system continues in domain D_J under the corresponding dynamics defined by F_J . The flow $\phi(t, t_0, x_0, U)$ describes how the hybrid system evolves from some initial time t_0 and state x_0 until some final time t under input sequence U .

B. Underactuated Systems

Following the definition in [25, Ch. 1.2], a system with state $x = [q, \dot{q}]^T$ and dynamics $\dot{q} = F(t, x(t), u(t))$ is underactuated if for all q, \dot{q} , and t , $F : u \mapsto \ddot{q}$ is not surjective, i.e there exists a \ddot{q} that can not be commanded by any u . For hybrid systems, we classify a domain with the above property as an underactuated domain, and any hybrid system with at least one underactuated domain as an underactuated hybrid system.

Even when an underactuated domain is controllable, driving the system to a desired target state may require significant time and control effort, neither of which may be readily available. For instance, a robot jumping in the air can not arbitrarily choose how much time it will have until its feet touchdown on the ground. In general, common optimal control techniques like the linear quadratic regulator (LQR) can only guarantee stability after a sufficiently long time, and may not reduce errors in all directions across a time-constrained domain. For a jumping robot, this means that if touchdown occurs too soon, errors in certain directions may have increased across the aerial domain. This is exacerbated by discontinuous, unbounded saltation effects that can cause arbitrarily large divergence if incoming errors are not sufficiently mitigated.

While difficult, it is possible to control underactuated hybrid systems with carefully designed trajectories and feedback controllers. Increasing controller gains is one possible solution to improving stability, though that strategy comes at a large drawback of worsening robustness in the face of modelling errors and uncertainties [26, Ch. 13]. Instead, this work leverages the fact that nonlinearities in continuous and hybrid dynamics make some trajectories easier to stabilize than others, even under equivalent feedback controllers.

III. ANALYSIS AND PLANING FOR HYBRID SYSTEMS

With the understanding that underactuated hybrid systems are challenging to control, we now set out to quantify the performance of a closed-loop hybrid trajectory using linearized variational equations. With this analysis, we can generate a scalar measure of a trajectory's convergence which is then incorporated into a trajectory optimization framework.

A. Linearized Variational Equations

For both continuous domains and hybrid transitions, linearized variational equations can be constructed to characterize the evolution of perturbations δx [27]. In each continuous

domain, the linearized variational equation is discretized from timestep i to $i + 1$ and is equivalent to the standard form of continuous system dynamics, $\delta x_{i+1} \approx A_I \delta x_i + B_I u_i$ [27] with A_I and B_I being the derivatives of the discretized dynamics in mode I w.r.t. state x_i and control inputs u_i , respectively. For hybrid events, the analogous variational equation is the saltation matrix $\Xi_{(I,J)}$, which describes the transition between modes I and J. The saltation matrix is the first-order approximation of the change in state perturbations from before the hybrid event at $\delta x(t^-)$ to perturbations after $\delta x(t^+)$ [20], such that:

$$\delta x(t^+) \approx \Xi_{(I,J)} \delta x(t^-) \quad (1)$$

Adapting the formulation from [28,29], the saltation matrix is:

$$\Xi_{(I,J)} = D_x R + \frac{(F_J^+ - D_x R \cdot F_I^- - D_t R) D_x g}{D_t g + D_x g F_I^-} \quad (2)$$

where:

$$R := R_{(I,J)}(t^-, x(t^-), u(t^-)), \quad g := g_{(I,J)}(t^-, x(t^-), u(t^-)), \\ F_I^- := F_I(t^-, x(t^-), u(t^-)), \quad F_J^+ := F_J(t^+, x(t^+), u(t^+))$$

B. Convergence Measure

Consider a trajectory that begins at state $x_0 = x(t_0)$ for some initial time t_0 and is executed until time t_f where it arrives at state $x_f = \phi(t_f, t_0, x_0, U)$. Our control objective is to bring any nearby initial state $\bar{x}_0 = x_0 + \delta x_0$ towards the nominal trajectory so that $\bar{x}_f = \phi(t_f, t_0, \bar{x}_0, \bar{U}) = x_f + \delta x_f$ is sufficiently “close” to x_f . To characterize the closeness of \bar{x}_f and x_f , we utilize the fundamental solution matrix, Φ . Following [30], the fundamental solution matrix is:

$$\Phi = \frac{\partial \phi(t_f, t_0, x_0, U)}{\partial x_0} \quad (3)$$

such that to the first order, $\delta x_f \approx \Phi \delta x_0$. Φ is the non-periodic generalization of the monodromy matrix that has been used to study periodic trajectories [21,30].

The fundamental solution matrix can be computed by sequentially composing the linearized variational equations in each continuous domain ($\dot{A} := A - BK$ for domains with linear feedback control) and the saltation matrices (Ξ) at each hybrid event [21]. For a hybrid trajectory with N domains, the fundamental solution matrix can be formulated as:

$$\Phi = \tilde{A}_N \dots \Xi_{(2,3)} \tilde{A}_2 \Xi_{(1,2)} \tilde{A}_1 \quad (4)$$

Since the fundamental solution matrix captures the change in errors across a trajectory, the singular values of Φ characterize error change along principle axes of state space. The largest singular value, which is equivalent to the induced 2-norm of Φ , describes the evolution of the most divergent direction of initial error δx_0 . We define the convergence measure, χ to be exactly this worst-case value:

$$\chi = \|\Phi\|_2 \quad (5)$$

χ is a continuous measure of local convergence, where smaller values of χ indicate stronger reduction of worst-case final errors. A value of $\chi < 1$ indicates errors in all directions will shrink.

C. iLQR for Hybrid Systems

Trajectory optimization for legged robots is a rich field that has been receiving steadily increasing attention [31]. One difficulty in designing legged robot trajectories is selecting an appropriate gait sequence and many methods rely on a fixed, predefined gait sequence [32,33]. While these strategies work well in situations where the ideal gait sequence is obvious (bipedal left-right alternating walking), additional legs and complex environments make this problem non-trivial. We draw from recent work [34], where the hybrid iLQR algorithm is able to alter and optimize the gait sequence.

In brief, iLQR solves the optimal control problem over N timesteps:

$$\min_U \ell_N(x_N) + \sum_{i=0}^{N-1} \ell_i(x_i, u_i) \quad (6)$$

$$\text{where } x_0 = x(0) \quad (7)$$

$$x_{i+1} = \phi(t_{i+1}, t_i, x_i, u_i) \quad \forall i \quad (8)$$

where $X := \{x_0, x_1, \dots, x_N\}$ is a sequence of states with $x_i \in \mathbb{R}^n$ the system state at timestep i and $U := \{u_0, u_1, \dots, u_{N-1}\}$ is a sequence of control inputs with $u_i \in \mathbb{R}^m$ the control input at timestep i . We also record the sequence of domains $M := \{D_0, D_1, \dots, D_N\}$ with $D_i \in \mathcal{D}$ the domain at timestep i such that $x_i \in D_i$. ϕ is the aforementioned flow of the trajectory, encompassing both the continuous dynamics in the individual modes and the reset maps between them.

iLQR makes a quadratic approximation of the cost function, where the cost terms can be simplified as:

$$\ell_N = x_N^T Q_N x_N \quad (9)$$

$$\ell_i = x_i^T Q_i x_i + u_i^T R_i u_i \quad (10)$$

and the approximation of the cost function as:

$$J = x_N^T Q_N x_N + \sum_{i=0}^{N-1} x_i^T Q_i x_i + u_i^T R_i u_i \quad (11)$$

with $Q_i, Q_N \in \mathbb{R}^{n \times n}$ and $R_i \in \mathbb{R}^{m \times m}$ all positive definite.

iLQR solves the optimal control problem by alternating between forward passes that simulate the system under a given control input sequence, and backward passes that solve for a new locally optimal control sequence. In the backward pass, the value function \mathcal{V} , which is the optimal cost to go at any timestep, is propagated through the trajectory in reverse, which gives locally optimal feedforward inputs and feedback gains at each timestep. Computing the value function relies on gradient and Hessian computations of the cost function and Jacobians of the dynamics, which are denoted ϕ_x and ϕ_u , where subscripts indicate differentiation w.r.t. the subscripted variable. For timesteps that do not undergo any hybrid events, the dynamics Jacobians are the familiar $\phi_x = A$ and $\phi_u = B$ linearizations of continuous systems. The saltation matrix is inserted into the dynamics Jacobians for timesteps where a hybrid event occurs, such that $\phi_x = \Xi A$ and $\phi_u = \Xi B$. We assume that each timestep has a maximum of one hybrid event occur.

The value function expansions, which are used to compute the feedforward inputs and feedback gains at each timestep as well as the next value function iteration, are written as:

$$Q_{xx} = J_{xx} + \phi_x^T \mathcal{V}_{xx} \phi_x \quad (12)$$

$$Q_{uu} = J_{uu} + \phi_u^T \mathcal{V}_{xx} \phi_u \quad (13)$$

$$Q_{ux} = J_{ux} + \phi_u^T \mathcal{V}_{xx} \phi_x \quad (14)$$

$$Q_x = J_x + \phi_x^T \mathcal{V}_x \quad (15)$$

$$Q_u = J_u + \phi_u^T \mathcal{V}_x \quad (16)$$

For much greater detail of iLQR for hybrid systems, see [34].

IV. CONVERGENT iLQR

Here we present a novel trajectory optimization algorithm called convergent iLQR or χ -iLQR. To do this, we add the convergence measure into the cost function from (11) such that the algorithm minimizes:

$$J_\chi = Q_\chi \chi + x_N^T Q_N x_N + \sum_{i=0}^{N-1} x_i^T Q_i x_i + u_i^T R_i u_i \quad (17)$$

where Q_χ is a scalar weighting parameter.

A challenge that arises when solving this new cost function is the dependence of the convergence measure on the controller feedback gains. Typically in iLQR, the cost function J is evaluated after each forward pass, since it is only dependent on the states and inputs of the most recent trajectory. However, in this case the convergence measure portion of the cost function is dependent on the feedback gains generated by the algorithm. This means that the gradient and Hessian terms of the cost function rely on the feedback gains that are being updated at every timestep in the backward pass. Due to this, the cost function derivatives are highly coupled with the gains and become convoluted to compute.

To resolve this, we propose executing two separate backward passes that each compute a different set of gains. The tracking backward pass computes the feedback gains that will be used as the LQR tracking controller gains and to compute the convergence measure. This tracking backward pass is equivalent to the backward pass in the standard iLQR algorithm using the cost function J (11), solving the Riccati equation for the most recent trajectory. With the gains generated in the tracking backward pass K_t , the convergent cost function J_χ (17) be computed. The search backward pass takes J_χ from the tracking backward pass and computes the gradients of the convergent cost function with controller gains K_t . The feedforward inputs k_s and the feedback gains K_s from this pass is used to search for an improved trajectory in the forward pass. The χ -iLQR algorithm is shown in Algorithm 1.

In standard iLQR, a line search is performed within the forward pass to guarantee the reduction of the cost function after every iteration. Here, since J_χ is returned by the tracking backward pass, the line search is performed after this function call to evaluate the reduction of J_χ . If the line search condition is not satisfied, the forward pass and

Algorithm 1 Convergent iLQR Algorithm

```

Initialize  $U, Q_\chi, Q_N, Q_i, R_i, n_{\text{iterations}}$ 
 $X, U, M, J \leftarrow \text{ROLLOUT}(U)$ 
 $K_t, J_\chi \leftarrow \text{TRACKINGBACKWARDPASS}(X, U, M, J)$ 
for  $i \leftarrow 1$  to  $n_{\text{iterations}}$  do
   $k_s, K_s \leftarrow \text{SEARCHBACKWARDPASS}(X, U, M, J_\chi)$ 
  repeat
     $X, U, M, J \leftarrow \text{FORWARDPASS}(X, U, M, k_s, K_s)$ 
     $K_t, J_\chi \leftarrow \text{TRACKINGBACKWARDPASS}(X, U, M, J)$ 
  until  $\text{LINESEARCHISSATISFIED}(J_\chi)$ 
return  $X, U, M, K_t$ 

```

tracking backward pass are looped until the line search is condition is passed.

Within the search backward pass, iLQR requires computation of the gradient and Hessian of χ . Assuming all elements of Φ are continuously differentiable with respect to state, χ is also continuously differentiable [35]. Because the scalar χ is derived from the norm of the matrix Φ , the gradient of χ relies on computing a 3-dimensional tensor of Φ derivatives, and the Hessian of χ is computed from a 4-dimensional tensor of Φ second derivatives. While recent work has enabled faster computation of second derivatives of dynamics [36] which can aid in the computation of the 3-D tensor derivatives, computing 4-D tensor derivatives is generally untenable. Instead, numerical methods like finite differences for gradients and BFGS [37] for Hessians can perform at reasonable, though not real-time, speed.

V. EXAMPLES AND RESULTS

In this section, we demonstrate the convergence improvements of our method on a simple spring hopper system and a planar quadruped robot model. Simulation results show that the improved convergence measure correlates with an improvement in average tracking performance, robustness to large disturbances, and feedback control effort. Both examples were implemented in MATLAB, with forward simulations using the `ode113` function. Cost function gradients were computed using finite differences and Hessians with BFGS.

A. Rocket Hopper

1) *Rocket Hopper Model*: The rocket hopper model is made up of a point mass body with a single massless spring leg. The state of the hopper is characterized by the positions x_B, y_B of the body, the angle θ of the leg and their derivatives $\dot{x}_B, \dot{y}_B, \dot{\theta}$ such that the full state is the 6×1 vector:

$$x = [x_B \quad y_B \quad \theta \quad \dot{x}_B \quad \dot{y}_B \quad \dot{\theta}]^T \quad (18)$$

The system has two domains: an aerial phase D_1 where the foot is above the ground and a stance phase D_2 where the foot is in contact with the ground. Taking a constant ground height at zero gives a touchdown guard function $g_{(1,2)}$ that is the height of the foot and a liftoff guard function $g_{(2,1)}$ that is the ground reaction force applied by the spring leg. Both

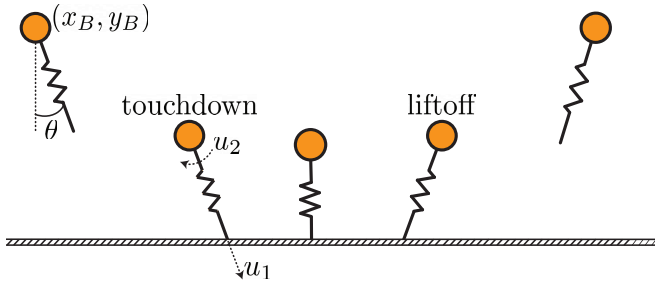


Fig. 2. Rocket hopper with actuation at the hip end of the leg.

reset maps $R_{(1,2)}$ and $R_{(2,1)}$ are identity since the position and velocity of the body and leg angle are continuous. At touchdown, the x-position of the foot is stored in order to compute the constrained spring dynamics in stance.

We equip the hopper model with two inputs: a hip actuation and an actuation in the direction of the leg. In the air, this allows the hopper to rotate the leg around the body and exert a propulsion in the direction of the leg, somewhat akin to a rocket, though this force can approximate forces from other legs or actuators. In the air, we include a small rotor inertia that is removed in stance to ensure the dynamics are well-conditioned when controlling the massless leg. In stance, the hip torque and rocket force exert ground reaction forces on the body. Fig. 2 summarizes the hopper model state and inputs. The physical properties of the hopper are chosen as a body mass of 1 kg, a spring constant of 250 N/m, and a resting leg length of 0.75 m.

2) *Rocket Hopper Results*: The objective for this system is to begin in the air at rest with a height of 2 m and end in the air at rest with the same height displaced 0.2 m horizontally. The system is given 1.5 s for this trajectory.

We generated four trials of paired trajectories with varied weighting parameters shown in Table I and compared the performance of the standard (vanilla) iLQR method (where $Q_\chi = 0$) to χ -iLQR. There is no reference trajectory to track, so Q_i is zero for all trials. Note in Table I, 0 represents the 6×6 zero matrix. To demonstrate the ability to have mode-dependent gains, and because actuation on the ground is expected to be more expensive than in the air due to the change in inertia of the dynamics model, we use an input cost $R_{i_{\text{air}}}$ for timesteps in the aerial domain, and a higher input cost $R_{i_{\text{stance}}}$ for timesteps that are in stance.

For 3 of these trials, the vanilla hybrid iLQR generated a trajectory with $\chi > 1$, meaning the worst-case error direction was expansive, see Table II. χ -iLQR decreases every con-

TABLE I
CONTROL WEIGHTS FOR ROCKET HOPPER TESTING

Trial	Q_χ	Q_N	Q_i	$R_{i_{\text{air}}}$	$R_{i_{\text{stance}}}$
1	50	500 I	0	$10^{-2} I$	$10^{-1} I$
2	50	800 I	0	$5 \cdot 10^{-3} I$	$10^{-2} I$
3	50	250 I	0	$2 \cdot 10^{-2} I$	$5 \cdot 10^{-2} I$
4	75	500 I	0	$10^{-2} I$	$10^{-2} I$

vergence measure to below 1 so that all error directions are reduced over the trajectory. On average, χ -iLQR decreased χ by 28.79% compared to the vanilla method.

To validate these generated trajectories, each closed-loop trajectory was simulated 100 times with small random initial perturbations in both positions and velocities with covariance matrix $\text{cov}(X_0) = 10^{-4} I$. A small covariance was chosen so that the linearizations assumed in the convergence measure and LQR control are valid. For each simulation run, the initial error δx_0 and the final error δx_f were recorded, along with the sequence of control inputs $V := \{v_0, v_1, \dots, v_{N-1}\}$. Note that these inputs are distinct from the nominal feed-forward inputs to the system U because there is additional feedback effort exerted by the actuators. The same set of initial errors was used to test both trajectories.

Two values were recorded during each simulation run to characterize the convergence properties of the trajectories. The first is the error ratio, E defined as the ratio of the final error 2-norm to the initial error 2-norm:

$$E = \frac{\|\delta x_f\|_2}{\|\delta x_0\|_2} \quad (19)$$

A lower error ratio means better tracking performance, and $E < 1$ indicates a net reduction in error. The second value is the feedback effort, F which is the sum of squares of the difference between V and U :

$$F = \sum_{i=0}^{N-1} (v_i - u_i)^2 \quad (20)$$

Table II shows that the simulation results support our assertion that an improved convergence measure correlates with an improved mean tracking performance and feedback effort. The mean error ratio and feedback effort over the 100 simulations were both lower for trajectories generated with χ -iLQR. The average improvement over the four trials was 19.30% for mean error ratio and 13.17% for feedback effort.

None of the simulated runs had an error ratio greater than one, which is sensible since the worst-case direction occurs with probability zero. However, even if none of the sampled initial errors aligned exactly with the worst-case direction predicted by the fundamental solution matrix, nearby initial error directions still see improvement in convergence, which explains the improvement in mean simulated error ratio.

B. Planar Quadruped

Here we demonstrate the improvements of χ -iLQR on a more complex robot model akin to the quadruped robot, Ghost Robotics Spirit 40. The model is simplified as a planar quadruped, meaning that all movement occurs in the sagittal plane and the left-right pairs of legs are constrained to move identically.

1) *Planar Quadruped Model*: In the sagittal plane, we can model the robot with 7 positional states. x_B, y_B, θ_B characterize the position and orientation of the body. The front and back sets of legs each have two states for the hip

TABLE II
ROCKET HOPPER CONVERGENCE MEASURE AND SIMULATION RESULTS

Trial	Convergence Measure			Mean Simulated Error Ratio			Mean Simulated Feedback Effort		
	Vanilla	χ -iLQR	%Difference	Vanilla	χ -iLQR	%Difference	Vanilla	χ -iLQR	%Difference
1	1.01	0.71	-29.70%	0.42	0.33	-21.72%	$1.74 \cdot 10^{-5}$	$1.610 \cdot 10^{-5}$	-7.16%
2	0.78	0.51	-34.50%	0.32	0.24	-25.74%	$4.66 \cdot 10^{-5}$	$3.25 \cdot 10^{-5}$	-30.31%
3	1.14	0.94	-17.70%	0.49	0.45	-8.00%	$7.12 \cdot 10^{-6}$	$7.05 \cdot 10^{-6}$	-1.01%
4	1.01	0.68	-33.24%	0.41	0.32	-21.73%	$1.89 \cdot 10^{-5}$	$1.62 \cdot 10^{-5}$	-14.20%

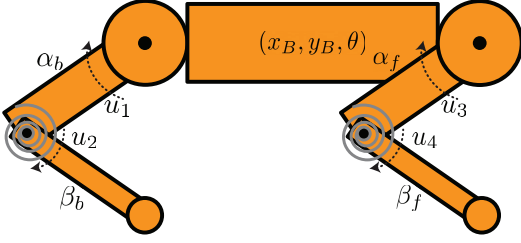


Fig. 3. The planar quadruped model with parallel torsion springs at knees.

angle α_f, α_b and knee angle β_f, β_b . Thus the configuration q is:

$$q = [x_B \ y_B \ \theta_B \ \alpha_f \ \alpha_b \ \beta_f \ \beta_b]^T \quad (21)$$

such that the full state, $x = [q^T \ \dot{q}^T]^T$ is the configuration q and its velocities \dot{q} .

This system has four domains: the aerial domain D_1 , the front stance domain D_2 where the front foot is on the ground and the back foot is in the air, the back stance domain D_3 , and the double stance domain D_4 where both feet are on the ground. Transitions can occur between any pair of domains since feet can transition simultaneously. Like the hopper system, the impact guard function that connects a foot's aerial domain to stance domain is the height of the foot and the guard function for liftoff is the vertical ground reaction force on that leg. The dynamics of the robot body in the aerial phase follows ballistic motion, while the legs are simplified to be massless while including the aforementioned rotor inertia. The impact reset map for each foot consists of a discrete update to the hip and knee velocities, while the body states are unchanged due to the massless legs. The reset map at liftoff is identity. The input vector for this system is 4-dimensional to actuate the hip and knee joints.

In this model, parallel torsion springs are added to the knee joints. Parallel joint springs have been utilized to mimic tendons found in animals [38] that increase the energy efficiency of legged locomotion [39,40]. Series elasticity is a similar way that spring dynamics have been incorporated in robots [41]. While not presented in this work, we anticipate χ -iLQR being similarly useful for these cases.

Due to the resonance of the natural spring dynamics, controlling these systems requires special care [42,43]. For example, [44] solved for optimal gait timings to leverage resonant spring frequencies. These spring models of legged

robots are good candidates for χ -iLQR because the dynamics of the stance phase depend strongly on the leg configuration at touchdown. Thus, a small error in leg states at touchdown can have a large effect on tracking performance.

Fig. 3 shows the planar quadruped model, where the inertial and dimensional properties were chosen to match the Ghost Robotics Spirit 40 quadruped. The added torsional knee spring has a spring constant $75 \text{ N} \cdot \text{m} \cdot \text{rad}^{-1}$ and rest angle 1.2 rad.

2) *Planar Quadruped Results*: The trajectory optimization task for the planar quadruped is to generate a gait with a forward velocity of 0.25 m/s. Like the hopper trajectory, the robot begins in the air with a body height of 0.3 m. The hip joints begin at an angle of 0.6 rad and the knee joints begin at the spring rest angle 1.2 rad. The initial configuration and velocity vectors are:

$$q_0 = [0 \ 0.3 \ 0 \ 0.6 \ 1.2 \ 0.6 \ 1.2]^T \quad (22)$$

$$\dot{q}_0 = [0.25 \ 0 \ 0 \ 0 \ 0 \ 0 \ 0]^T \quad (23)$$

We ask for a terminal target state that is equivalent to the initial state, but translated 0.0875 m in the positive x-direction. The trajectory is given 0.35 s to execute.

Like the previous example, the Q_i weighting matrix is set to zero. Here, we choose to set a constant input weight of $R_i = 5 \cdot 10^{-4} I$, though it is possible to select different sets of weights for the aerial and stance domains of each leg. The terminal weight is $Q_N = 500I$ and the convergence weight for χ -iLQR is $Q_\chi = 1$. From these weightings, we generate a vanilla iLQR trajectory and χ -iLQR trajectory.

We set up a similar experiment to the prior example, with the addition of simulating over a range of covariance magnitudes. This is done to evaluate the basin of attraction of each trajectory over larger initial errors that introduce greater nonlinear effects. The trajectories were evaluated with 6 sets of 100 paired simulation runs with random initial error covariance magnitudes of 10^{-4} , $5 \cdot 10^{-4}$, 10^{-3} , $5 \cdot 10^{-3}$, 10^{-2} , and $5 \cdot 10^{-2}$ in each direction. The lowest covariance magnitude of 10^{-4} approximates local linear behavior well, while $5 \cdot 10^{-2}$ is the maximum magnitude before some trials begin with the robot's feet below the ground.

Table III shows the nominal cost, convergence measure, mean simulated error ratio, and mean simulated feedback effort of the two trajectories at the smallest covariance magnitude 10^{-4} . The nominal cost of the convergent trajectory

TABLE III

CONVERGENCE RESULTS FOR THE QUADRUPEL MODEL OVER 100 TRIALS FOR VANILLA AND χ -iLQR TRAJECTORIES WITH COVARIANCE MAGNITUDE 10^{-4}

	Vanilla	χ -iLQR	%Difference
Nominal Cost	65.58	74.39	+13.43%
Convergence Measure	60.52	41.35	-31.68%
Mean Simulated Error Ratio	6.66	4.78	-28.23%
Mean Simulated Feedback Effort	0.016	0.013	-16.56%

increases, which is expected due to the additional cost terms the algorithm optimizes for. To offset this, the improvements in the convergence measure and simulation values are apparent. We believe this trade off between nominal cost and the convergence performance of the trajectory is a valuable tool for roboticists to have access to and tune appropriately.

The mean simulated error ratio for the convergent trajectory at this small covariance magnitude was 28.23% less and the mean simulated feedback effort was 16.56% less. Fig. 4 displays a histogram of the error ratio for each of the trials, and shows the improvement made by the convergent trajectory. Like the previous example, the likelihood of an initial error being aligned with the worst-case direction occurs with probability zero, and is especially unlikely with a larger state dimension of 14. Still, the correlations between convergence measure and mean tracking performance are reinforced.

As the magnitude of initial errors grows, the performance of the LQR tracking controller becomes worse due to the increase in unaccounted nonlinear effects. Fig. 5 shows the simulation results for each trajectory over a range of initial error covariance magnitudes. Each pair of lines indicates the success rate of the respective closed-loop trajectories at maintaining error ratios of less than 50, 10, and 5 respectively. An error ratio of greater than 50 is representative of a catastrophic failure, which the vanilla trajectory encounters at a covariance magnitude of $5 \cdot 10^{-4}$, while the convergent trajectory first experiences a failure at covariance magnitude 10^{-2} . This stark difference in performance suggests the convergent trajectory is more robust to larger initial errors and nonlinearities. Fig. 1 displays the tracking performance improvement of χ -iLQR at the larger 10^{-2} covariance magnitude. At this covariance magnitude, the mean simulated error ratio of the vanilla trajectory was 127.39, whereas for the convergent trajectory it was 9.62, a 92% improvement.

Even with the convergence improvements in the χ -iLQR trajectory, the controller is still not able to reduce errors in all directions. In fact, the simulation results found that most of the time, there was some growth in error. This indicates that controlling this system is exceedingly difficult, which is reasonable since the body dynamics are fully unactuated in the aerial phase and the system undergoes multiple hybrid events. A combination of higher feedback gains and a more global footstep planner could be able to grant this system full convergence. Even so, this work can be valuable to

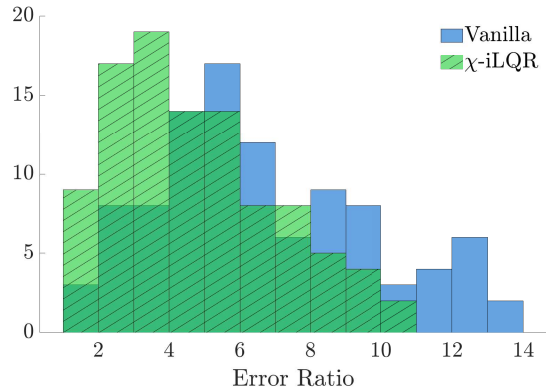


Fig. 4. Histogram of error ratio for 100 paired simulated trials of the quadruped model with small initial perturbations of covariance magnitude 10^{-4} . Error ratio is the 2-norm of final errors divided by the 2-norm of initial errors.

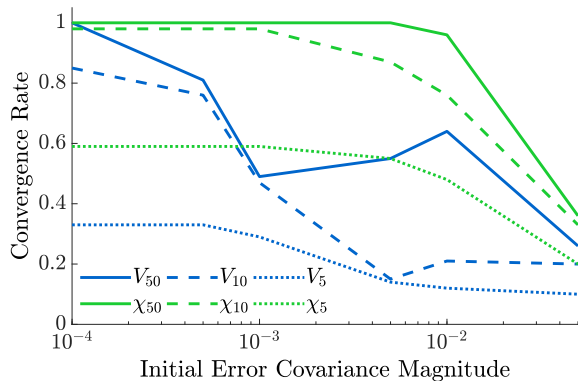


Fig. 5. Plots showing success of LQR controllers at tracking vanilla and convergent trajectories over various initial perturbation covariances. V_{50} and χ_{50} indicate proportion of trials where error ratio was below 50, V_{10} and χ_{10} below 10, and V_5 and χ_5 below 5.

ensure that between iterations of a global footstep planner, the closed-loop system does not diverge too far from its target trajectory and experience a failure, such as falling over.

VI. CONCLUSION

In this work, we present a novel trajectory optimization method, χ -iLQR that optimizes over the worst-case error growth of a hybrid trajectory. This method is based on the fundamental solution matrix, which maps the evolution of perturbations through a trajectory. Incorporating the saltation matrix into the fundamental solution matrix allows for straightforward handling of hybrid events. The simulation results presented on two legged robot models demonstrate that this method simultaneously produces trajectories with improved tracking performance, decreased feedback actuation effort, and improved robustness to large perturbations. Even for a quadrupedal trajectory that was very difficult to track, χ -iLQR produced a trajectory that was superior at avoiding failure outcomes.

Following up on this work, we aim to apply these principles to robot hardware and demonstrate stable and robust

performance for a variety of maneuvers such as leaping, pronking, and flipping. We also aim to apply this work to other classes of hybrid systems, such as robots that undergo slip-stick and stick-slip transitions at their feet or wheels. This work and its extensions will further enable robots to navigate complex, uncertain environments and unlock more worlds for robots to explore.

REFERENCES

- [1] M. Chignoli, S. Morozov, and S. Kim, "Rapid and reliable quadruped motion planning with omnidirectional jumping," *IEEE International Conference on Robotics and Automation*, 2022.
- [2] H. Kolvenbach, E. Hampp, P. Barton *et al.*, "Towards jumping locomotion for quadruped robots on the moon," *IEEE/RSJ International Conference on Intelligent Robots and Systems*, 2019.
- [3] C. Nguyen and Q. Nguyen, "Contact-timing and trajectory optimization for 3d jumping on quadruped robots," *IEEE/RSJ International Conference on Intelligent Robots and Systems*, 2022.
- [4] Z. Li, X. B. Peng, P. Abbeel *et al.*, "Robust and versatile bipedal jumping control through multi-task reinforcement learning," *arXiv preprint arXiv:2302.09450*, 2023.
- [5] J. Norby, A. Tajbakhsh, Y. Yang, and A. M. Johnson, "Adaptive complexity model predictive control," *arXiv preprint arXiv:2209.02849*, 2022.
- [6] Z. Manchester and S. Kuindersma, "Robust direct trajectory optimization using approximate invariant funnels," *Auton. Robots*, 2019.
- [7] J. Morimoto, G. Zeglin, and C. Atkeson, "Minimax differential dynamic programming: application to a biped walking robot," *IEEE/RSJ International Conference on Intelligent Robots and Systems*, 2003.
- [8] T. Lew, R. Bonalli, and M. Pavone, "Chance-constrained sequential convex programming for robust trajectory optimization," *European Control Conference*, 2020.
- [9] B. Hammoud, M. Khadiv, and L. Righetti, "Impedance optimization for uncertain contact interactions through risk sensitive optimal control," *IEEE Robotics and Automation Letters*, 2021.
- [10] M. Ahmadi, X. Xiong, and A. D. Ames, "Risk-sensitive path planning via CVaR barrier functions: Application to bipedal locomotion," *IEEE Control Systems Letters*, 2021.
- [11] L. Drnach and Y. Zhao, "Robust trajectory optimization over uncertain terrain with stochastic complementarity," *IEEE Robotics and Automation Letters*, 2021.
- [12] S. Kousik, S. Vaskov, F. Bu *et al.*, "Bridging the gap between safety and real-time performance in receding-horizon trajectory design for mobile robots," *The International Journal of Robotics Research*, 2020.
- [13] H. Khalil, *Nonlinear Systems*. Pearson, 2002.
- [14] A. Papachristodoulou and S. Prajna, "On the construction of Lyapunov functions using the sum of squares decomposition," *IEEE Conference on Decision and Control*, 2002.
- [15] S. Chen, M. Fazlyab, M. Morari *et al.*, "Learning Lyapunov functions for hybrid systems," *International Conference on Hybrid Systems: Computation and Control*, 2021.
- [16] R. Grandia, A. J. Taylor, A. D. Ames, and M. Hutter, "Multi-layered safety for legged robots via control barrier functions and model predictive control," *IEEE International Conference on Robotics and Automation*, 2021.
- [17] W. Lohmiller and J. Slotine, "On contraction analysis for non-linear systems," *Automatica*, 1998.
- [18] A. M. Johnson, J. E. King, and S. Srinivasa, "Convergent planning," *IEEE Robotics and Automation Letters*, 2016.
- [19] N. J. Kong and A. M. Johnson, "Optimally convergent trajectories for navigation," *International Symposium on Robotics Research*, 2022.
- [20] S. A. Burden, T. Libby, and S. D. Coogan, "On contraction analysis for hybrid systems," *arXiv preprint arXiv:1811.03956*, 2018.
- [21] J. Zhu, N. Kong, G. Council, and A. Johnson, "Hybrid event shaping to stabilize periodic hybrid orbits," *IEEE International Conference on Robotics and Automation*, 2022.
- [22] A. van der Schaft and J. Schumacher, "Complementarity modeling of hybrid systems," *IEEE Transactions on Automatic Control*, 1998.
- [23] J. Lygeros, K. H. Johansson, S. Simic *et al.*, "Dynamical properties of hybrid automata," *IEEE Transactions on Automatic Control*, 2003.
- [24] A. M. Johnson, S. A. Burden, and D. E. Koditschek, "A hybrid systems model for simple manipulation and self-manipulation systems," *The International Journal of Robotics Research*, 2016.
- [25] R. Tedrake, *Underactuated Robotics*, 2022. [Online]. Available: <http://underactuated.mit.edu>
- [26] M. A. Haidekker, *Linear Feedback Controls*, M. A. Haidekker, Ed. Elsevier, 2020.
- [27] M. Hirsch, S. Smale, and R. Devaney, *Differential Equations, Dynamical Systems, and an Introduction to Chaos*. Academic Press, 2012.
- [28] S. A. Burden and S. D. Coogan, "On infinitesimal contraction analysis for hybrid systems," *IEEE Conference on Decision and Control*, 2022.
- [29] P. Müller, "Calculation of Lyapunov exponents for dynamic systems with discontinuities," *Chaos, Solitons & Fractals*, 1995.
- [30] R. Leine and H. Nijmeijer, *Dynamics and Bifurcations of Non-Smooth Mechanical Systems*. Springer-Verlag Berlin Heidelberg, 2004.
- [31] P. M. Wensing, M. Posa, Y. Hu *et al.*, "Optimization-based control for dynamic legged robots," *arXiv preprint arXiv:2211.11644*, 2022.
- [32] M. Posa, C. Cantu, and R. Tedrake, "A direct method for trajectory optimization of rigid bodies through contact," *The International Journal of Robotics Research*, 2014.
- [33] Z. Manchester, N. Doshi, R. J. Wood, and S. Kuindersma, "Contact-implicit trajectory optimization using variational integrators," *The International Journal of Robotics Research*, 2019.
- [34] N. J. Kong, G. Council, and A. M. Johnson, "ILQR for piecewise-smooth hybrid dynamical systems," *IEEE Conference on Decision and Control*, 2021.
- [35] K. Petersen and M. Pedersen, *The Matrix Cookbook*. Technical University of Denmark, 2012.
- [36] S. Singh, R. P. Russell, and P. M. Wensing, "On second-order derivatives of rigid-body dynamics: Theory & implementation," *arXiv preprint arXiv:2302.06001*, 2023.
- [37] C. G. Broyden, "The convergence of a class of double-rank minimization algorithms I. General considerations," *IMA Journal of Applied Mathematics*, 1970.
- [38] K. Endo and H. Herr, "A model of muscle-tendon function in human walking at self-selected speed," *IEEE Transactions on Neural Systems and Rehabilitation Engineering*, 2014.
- [39] M. Scheint, M. Sobotka, and M. Buss, "Optimized parallel joint springs in dynamic motion: Comparison of simulation and experiment," *IEEE RAS & EMBS International Conference on Biomedical Robotics and Biomechanics*, 2010.
- [40] K. Mombaur, "Using optimization to create self-stable human-like running," *Robotica*, 2009.
- [41] M. Hutter, C. Gehring, D. Jud *et al.*, "ANYmal - A highly mobile and dynamic quadrupedal robot," *IEEE/RSJ International Conference on Intelligent Robots and Systems*, 2016.
- [42] D. Lakatos, K. Ploeger, F. Loeffl *et al.*, "Dynamic locomotion gaits of a compliantly actuated quadruped with slip-like articulated legs embodied in the mechanical design," *IEEE Robotics and Automation Letters*, 2018.
- [43] J. Ackerman and J. Seipel, "Energy efficiency of legged robot locomotion with elastically suspended loads," *IEEE Transactions on Robotics*, 2013.
- [44] M. J. Pollayil, C. D. Santina, G. Mesesan *et al.*, "Planning natural locomotion for articulated soft quadrupeds," *IEEE International Conference on Robotics and Automation*, 2022.